

RelTriple: Learning Plausible Indoor Layouts by Integrating Relationship Triples into the Diffusion Process

Kaifan Sun^{1†}, Bingchen Yang^{1†}, Peter Wonka², Jun Xiao¹, Haiyong Jiang¹

¹ University of Chinese Academy of Sciences (UCAS)

² King Abdullah University of Science and Technology, KAUST

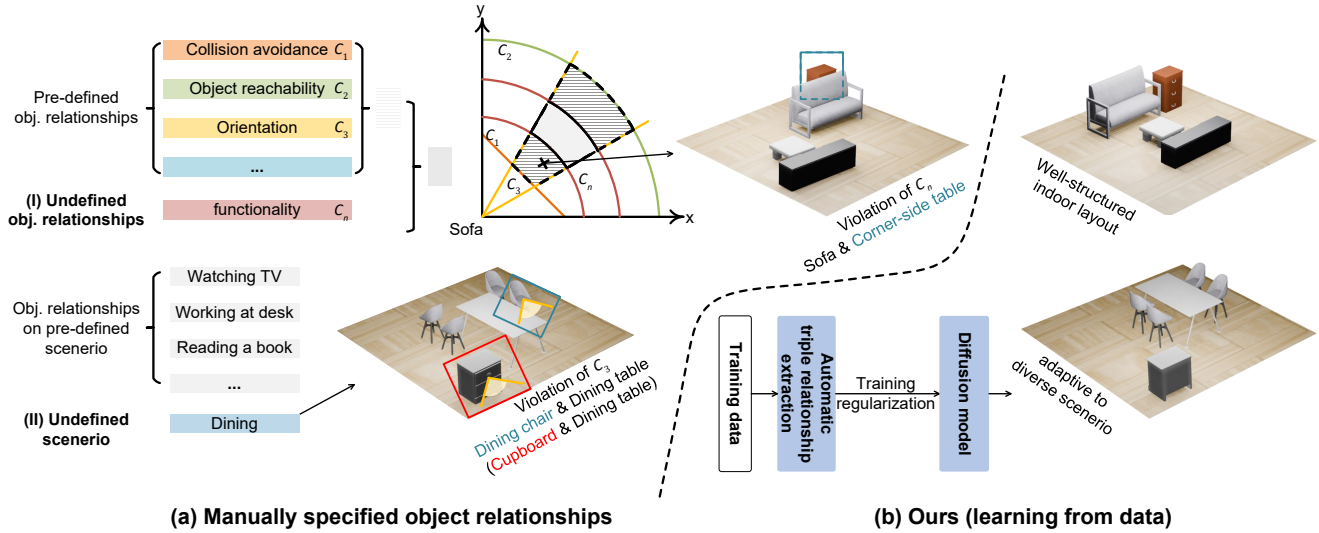


Figure 1. **Comparison of indoor layout synthesis methods:** (a) Manually specified constraints tend to be incomplete, resulting in unrealistic layout generation. (b) Data-driven constraint learning derives important spatial relationships automatically from the dataset, enabling the creation of well-organized layouts.

Abstract

The generation of indoor furniture layouts has significant applications in augmented reality, smart homes, and architectural design. Successful furniture arrangement requires proper physical relationships (e.g., collision avoidance) and spacing relationships between furniture and their functional zones to be respected. However, manually defined relationships are almost always incomplete and can produce unrealistic layouts. This work instead extracts spacing relationships automatically based on a hierarchical analysis and adopts the Delaunay Triangulation to produce important triple relationships. Compared to pairwise relationship modeling, triple relationships account for interactions and space utilization among multiple objects. To this end, we introduce RelTriple, a novel approach that enhances furniture distribution by learning spacing relation-

ships between objects and regions. We formulate triple relationships as object-to-object (O2O) losses and object-to-region (O2R) losses and integrate them directly into the training process of generative diffusion. Our approach consistently improves over existing state-of-the-art methods in visual results evaluation metrics on unconditional layout generation, floorplan-conditioned layout generation, and scene rearrangement, achieving at least 12% on the introduced spatial relationship metric and superior spatial coherence and practical usability.

1. Introduction

Automatically generating indoor layouts is critical for a range of applications, including virtual and augmented reality (VR/AR) [41], smart home systems [29], robotics [12], and interior designs [13]. The rise of generative models [30, 34, 48, 49] has unlocked new possibilities, sig-

[†] Equal contribution

nificantly advancing both quality and efficiency of indoor layout generation. Despite the progress, generating layouts with practical usability remains an open challenge. Achieving this requires respecting physical constraints, ergonomic rules, spacing, and other relationships.

Recent approaches [20, 24, 42, 44, 56] derive primary object relationships from expert knowledge to aid layout generation, such as collision avoidance [44, 56], object reachability [24, 56], and human behavior guidance [20, 42]. These object relationships are constructed and enforced as additional regularization [24, 44] and classifier guidance on a generative model [56]. However, most methods focus on specific relationships based on predefined rules and parameters. These relationships usually do not consider the proper spacing between objects and an object to a functional region. For example, Physcene [56] emphasizes collision avoidance and reachability, but there is no objective to maintain object spacing between functionally related objects. As shown in Fig. 1 (a), a sofa can be positioned too close to the corner-side table while far from the coffee table and TV stand. Another example, LayoutEnhancer [24], lacks spacing relations to floorplan boundary and functional regions, leading to boundary violation between objects and the wall. Moreover, category-wise relationship modeling, e.g., LayoutEnhancer, sometimes requires manual effort to determine affected objects by each relationship type and is not scalable.

In light of these problems, we directly learn object spacings from the training data as illustrated in Fig. 1 (b). The spacing between nearby objects within a functional region is usually important to ensure functional pathways and physical interactivity. In addition, the spacing between an object and functional region bounds can avoid boundary violations and unreasonable object positions. To facilitate automatic relationship extraction, we observe the furniture-functional region-layout hierarchy can partition objects within a layout and that the geometric properties of the Delaunay Triangulation can enable it to find semantically meaningful local relationships.

From another perspective, previous work [24, 44, 56] mainly models pairwise relationships between two objects. Therefore, it fails to capture potential interactions among more than three objects. A typical example is the kitchen work triangle [23] that addresses the efficiency between major work centers, including cooking, sink, and refrigerator. Therefore, triple relationships can consider interactions among three objects and constrain relative positions better.

We propose a novel framework, RelTriple, to render the two above-mentioned observations to integrate spatial relationships into a generative model. The overall pipeline of RelTriple is shown in Fig 2. First, we automatically extract important relationships from an input layout hierarchically. To capture higher-order interactions, we propose to extract

relationship sub-graphs. In our current implementation, we break down these subgraphs into relationship triplets in the form of triangles. Second, we propose two types of losses: object-to-object losses and object-to-region losses to enhance the extracted relationships during the training of the diffusion model. Our contributions can be summarized as follows.

- A method to automatically extract important object-to-object and object-to-region relationships from an input floorplan.
- A formulation and differentiable rendering-based implementation of losses to enhance the extracted relationships during the training of a diffusion model.
- Superior performance on established scene synthesis metrics and significant improvements (at least 12%) over existing methods on newly introduced spatial relationship metrics for three tasks.

2. Related work

Generative Models for Indoor Layout Synthesis. The success of generative models in image generations [35, 38] has encouraged likewise explorations in indoor furniture synthesis, including variational auto-encoder (VAE) based methods [17, 28, 60], GANs [1, 22, 54, 55], autoregressive models [25, 32–34, 37, 47, 48], and diffusion models [27, 44, 49, 56, 61]. An interesting trend [3, 9, 11, 16, 43, 46, 57] is to leverage autoregressive Large Language Models (LLMs) as visual scene planners, generating layouts as structured text programs. Diffusion-based methods [27, 44, 49, 56, 61] approach layout synthesis as an object set diffusion process modeling the probability of object attributes. Some interesting works [44, 49, 56, 61] also explore diffusion models for layout rearrangement, conditional and unconditional indoor scene synthesis. Compared to the methods above, this work focuses on modeling spatial relationships in layout generation.

Graph-based Relationship Learning for Indoor Layouts. Plausible indoor layouts are usually bounded with complex layout relationships [6], such as co-occurrence, functionality, feasible placement, and layout balance. One line of work abstracts layout relationships as a graph for graph-conditioned layout synthesis. The relation graph can be manually specified [7, 28, 50, 53, 60, 61] or generated [4, 17, 26, 27, 33, 47]. As previous work focuses on binary relationships between two objects, many important layout aspects, such as walkable space, collisions, and space for access, need to be separately modeled. Our results indicate that the proposed spatial triple relationships more naturally capture important layout aspects.

Relationship-based Optimization for Indoor Layouts. Another line of work enforces layout relationships with

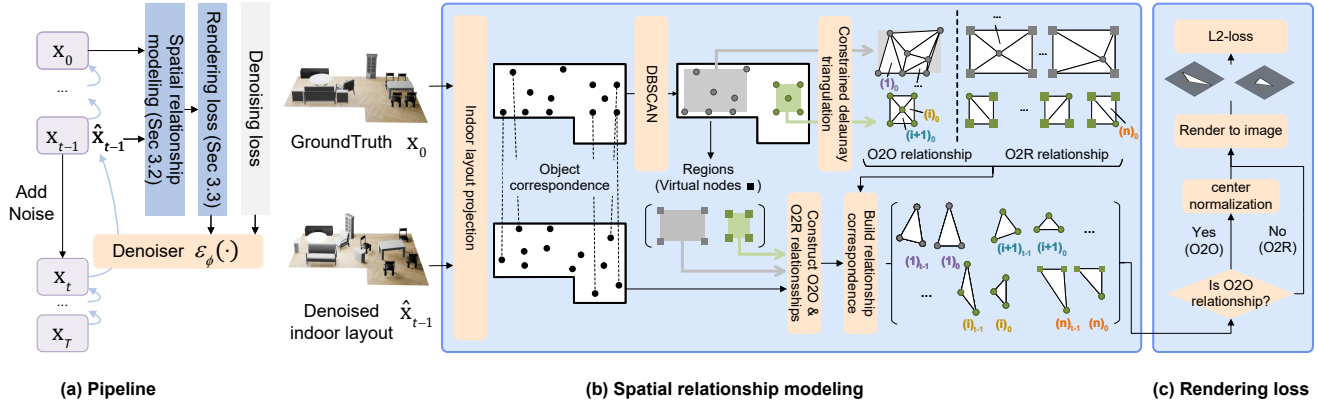


Figure 2. The overview of **RelTriple**. (a) We propose to automatically extract and model spatial relationships and integrate the relationships into the diffusion-based model training through a rendering loss. (b) We apply a hierarchical approach to identify important spatial relationships and corresponding losses. (c) The losses are evaluated through differentiable rendering.

gradient-based optimization. A typical strategy is to optimize a density function with Markov Chain Monte Carlo (MCMC) [31, 58, 59] and position-based dynamics [51, 62]. Another scheme incorporates additional relationships by deep reinforcement learning [42] and additional conditional guidance on deep generative models. PhyScene [56] and SHADE [20] adopt the classifier-guidance diffusion model [8] to optimize indoor layouts with collision avoidance and object reachability. LayoutEnhancer [24] introduces ergonomic rules as differentiable objective functions when training the generative model. Compared to relationship-wise formulation, our approach encodes object relationships using a unified triple representation, providing a concise form easily integrated with the rendering-based loss for effective optimization.

3. Method

This work aims to enhance the quality of indoor layout generation. To solve the problem, we introduce a geometric regularization term, RelTriple, to encode spatial relationships when training a diffusion model, as illustrated in Fig. 2. We start by introducing the preliminaries of our generative model in Sec. 3.1. In Sec. 3.2, we introduce how to extract spatial relationships from the indoor layout in a hierarchical manner. In Sec. 3.3, we present regularization terms and their implementation using differentiable rendering to better respect important spatial relationships in the generated layouts.

3.1. Preliminary

Our implementation is based on DiffuScene [44]. However, as demonstrated in experiments, it can be easily migrated to other indoor layout generative models.

Layout Representation. We encode an indoor layout \mathbf{x} as $\mathbf{x} = \{o_1, o_2, \dots, o_N\}$ with N objects, N varies for

different layouts. Each object o_i has a set of parameters $o_i = \{c_i, b_i, f_i\}$, where $c_i \in \mathbb{R}^C$ indicates its category within a set of C categories. $b_i = (s_i, p_i, r_i)$ is the 3D bounding box of the object o_i , defined by its size $s_i \in \mathbb{R}^3$, the coordinate of centroid $p_i \in \mathbb{R}^3$, and the ground plane orientation $r_i = (\cos \theta_i, \sin \theta_i) \in \mathbb{R}^2$. $f_i \in \mathbb{R}^{32}$ denotes a 3D object feature encoding the shape of the object.

Layout Diffusion. Starting with a clean indoor layout $\mathbf{x}_0 = \mathbf{x}$, we gradually add Gaussian noise through a forward diffusion process, transforming \mathbf{x}_0 into noisy data \mathbf{x}_T . This forward process consists of a series of transitions $q(\mathbf{x}_t | \mathbf{x}_{t-1})$ as follows:

$$q(\mathbf{x}_t | \mathbf{x}_{t-1}) = \mathcal{N}(\mathbf{x}_t; \sqrt{1 - \beta_t} \mathbf{x}_{t-1}, \beta_t \mathbf{I}) \quad (1)$$

β_t controls the noise variance at each time step. During the generative process, we gradually denoise noisy layout $\mathbf{x}_T \sim \mathcal{N}(0, \mathbf{I})$ with the reverse process $p(\mathbf{x}_{t-1} | \mathbf{x}_t)$. The reverse process is optimized by maximizing the log-likelihood of $p(\mathbf{x}_0)$

$$\mathcal{L}_{\text{diff}} = \mathbb{E}_{\mathbf{x}_0, \epsilon, t} [\|\epsilon - \epsilon_\phi(\mathbf{x}_t, t)\|_2^2], \quad (2)$$

where ϵ denotes the added Gaussian noise in each step, and $\epsilon_\phi(\mathbf{x}_t, t)$ is a denoising network. The denoising network $\epsilon_\phi(\mathbf{x}_t, t)$ adopts a UNet-1D module with self-attention [45].

Spatial Relationships. Due to the diversity of spatial relations, it is difficult to categorize spatial relations solely based on their intended semantic effects. RelTriple builds up object-to-object (O2O) and object-to-region (O2R) relationship categories based on the interacting components of the spatial relationship (See Fig. 2). O2O relationships encode local relationships between object triples. O2R relationships encode the spatial relationships of individual objects to layout regions.

3.2. Spatial Relationship Modeling

Given an initial indoor layout \mathbf{x} , we analyze the layout in a hierarchical manner to extract important regions in the layout and important spatial relationships between object triples within these regions. This process can be done as a one-time preprocessing step for each input layout in the dataset.

To start, we project the indoor layout onto the ground plane and represent objects as vertices. Since regional information is absent in the training data, we extract these regions using clustering and encode them as rectangular regions. Following SceneHGN [17], we utilize DBSCAN [10] to delineate object clusters based on the distance criteria between any two objects o_i, o_j as shown in Eq. 3,

$$m_{ij} = d_{ij} + \lambda_{\text{giou}} \cdot (1 - \text{GIoU}(b_i, b_j)), \quad (3)$$

where $\text{GIoU}(\cdot) \in [-1, 1]$ [36] takes into account the influence of bounding boxes b_i, b_j of two objects, and $d_{ij} = \|p_i - p_j\|_{xy}^2$ is the Euclidean distance between the centroids of the two objects on the ground plane. We define the regions as the bounding box of each cluster. The vertex coordinates of each region are derived from the maximum-minimum operator applied on the centroid coordinates of all objects within the cluster. We regard region vertices as virtual nodes, which differ from real objects because they have only centroid coordinates as effective attributes.

Next, we construct spatial relationship triplets by constructing triangles. We refer to the spatial proximity manipulation introduced in proximity compatibility principle [52], which suggests that spatially close objects are more likely to be related. We apply constrained Delaunay triangulation [5] to obtain a set of triangles M_{obj} . Delaunay triangulation not only provides a partition of the layout space, but its geometric properties also ensure the triangles are the most regular ones, thus avoiding meaningless triple relationships between an object and some other very faraway objects. Then, object-to-object relationships are encoded between real object triples, which are the three vertices of a triangle in the Delaunay triangulation. In this way, only objects that are close to each other have spatial relations. If a cluster contains only two objects, we add a virtual node to form an equilateral triangle.

We further connect each real object with the virtual objects and record them as object-to-region relationships. O2R relationships capture relative positions of furniture w.r.t. a region and connect the centroid of each piece of furniture to corners of the bounding box of a clustered region, forming four triangles. We denote these triangles as M_{reg} .

3.3. Loss Functions

Following PhyScene [56], we optimize the diffusion network with the regular diffusion loss in Eq. 2 and our newly

proposed losses to capture spatial relationships. Spatial relationships are constructed based on O2O and O2R triangles computed in the previous section. We denote the triangle for a predicted layout and a ground truth layout as \overline{M}_* and M_* , respectively. A neural renderer [21] can generate differential masks to allow for triangle-wise optimization between prediction and ground truths. We denote the rendering process as $\mathcal{R}(\cdot)$ with a triangle as input. Before calculating the loss for O2O triangles formed by three real objects, we first align a GT triangle and the corresponding predicted O2O triangle by translating their median points to the origin. This ensures the mask is translation-invariant and translation does not affect the relative spacing among objects of O2O triangles. We do not apply extra processing on O2O triangles, as the virtual nodes at different positions capture distinct regional contexts. Therefore, we have the object-to-object loss and object-to-region loss as follows:

$$\mathcal{L}_{\text{O2O}} = \frac{1}{|\overline{M}_{\text{obj}}|} \cdot \sum_{\substack{\overline{m}_i \in \overline{M}_{\text{obj}}, \\ m_i \in M_{\text{obj}}}} \|\mathcal{R}(\mathbf{c}(\overline{m}_i)) - \mathcal{R}(\mathbf{c}(m_i))\|_2, \quad (4)$$

$$\mathcal{L}_{\text{O2R}} = \frac{1}{|\overline{M}_{\text{reg}}|} \cdot \sum_{\substack{\overline{m}_i \in \overline{M}_{\text{reg}}, \\ m_i \in M_{\text{reg}}}} \|\mathcal{R}(\overline{m}_i) - \mathcal{R}(m_i)\|_2 \quad (5)$$

where $|\overline{M}_*|$ denotes the number of triangles within the set. $\mathbf{c}(\cdot)$ translates the centroid of a triangle to the origin for alignment. By introducing these losses, our method enhances the relationships extracted in the relationship modeling stage.

The overall optimization objective is a summation $\mathcal{L} = \mathcal{L}_{\text{diff}} + \lambda_{\text{O2O}}\mathcal{L}_{\text{O2O}} + \lambda_{\text{O2R}}\mathcal{L}_{\text{O2R}}$ with balancing weights λ_{O2O} and λ_{O2R} . To trade off the completeness of spatial relationship modeling and training efficiency, we randomly select five objects to compute their corresponding O2R triangles.

4. Results

4.1. Experimental Settings

Datasets. We train our model on the 3D-FRONT dataset [14], which consists of 6,813 houses and 14,629 rooms. Each room is furnished with high-quality items from the 3D-FUTURE dataset [15]. We utilize the same dataset as previous works [44, 56], containing 4,041 bedrooms, 900 dining rooms, and 813 living rooms. For each room type, 80% of the rooms are used for training, while the remaining are used for testing.

Metrics. To evaluate the visual quality of generated scenes, we follow Diffuscene [44] and employ perceptual similarity Fréchet Inception Distance (FID) [18], Kernel Inception Distance (KID $\times 0.001$) [2], Scene Classification Accuracy

Table 1. Quantitative comparisons on unconditioned layout generation.

Room	Method	FID↓	KID $\times 0.001$ ↓	SCA	CKL $\times 0.01$ ↓	Col _{obj} ↓	Col _{scene} ↓	D _{obj} ↓
Bedroom	ATISS	56.628	4.764	0.542	0.752	0.291	0.546	0.172
	LayoutEnhancer	42.515	4.241	0.523	0.526	0.256	0.488	0.108
	Diffuscene	39.422	4.352	0.527	0.396	0.247	0.462	0.072
	Ours	33.728	2.525	0.515	0.313	0.222	0.414	0.032
Living room	ATISS	74.522	5.671	0.592	0.511	0.384	0.878	0.672
	LayoutEnhancer	68.462	4.862	0.577	0.518	0.314	0.748	0.613
	Diffuscene	50.699	3.792	0.562	0.234	0.221	0.612	0.432
	Ours	46.216	0.982	0.513	0.218	0.146	0.468	0.222
Dining room	ATISS	72.433	5.524	0.586	0.653	0.422	0.806	0.581
	LayoutEnhancer	69.125	4.924	0.545	0.529	0.352	0.698	0.492
	Diffuscene	49.658	4.256	0.538	0.231	0.224	0.628	0.423
	Ours	47.321	1.464	0.522	0.213	0.184	0.540	0.208

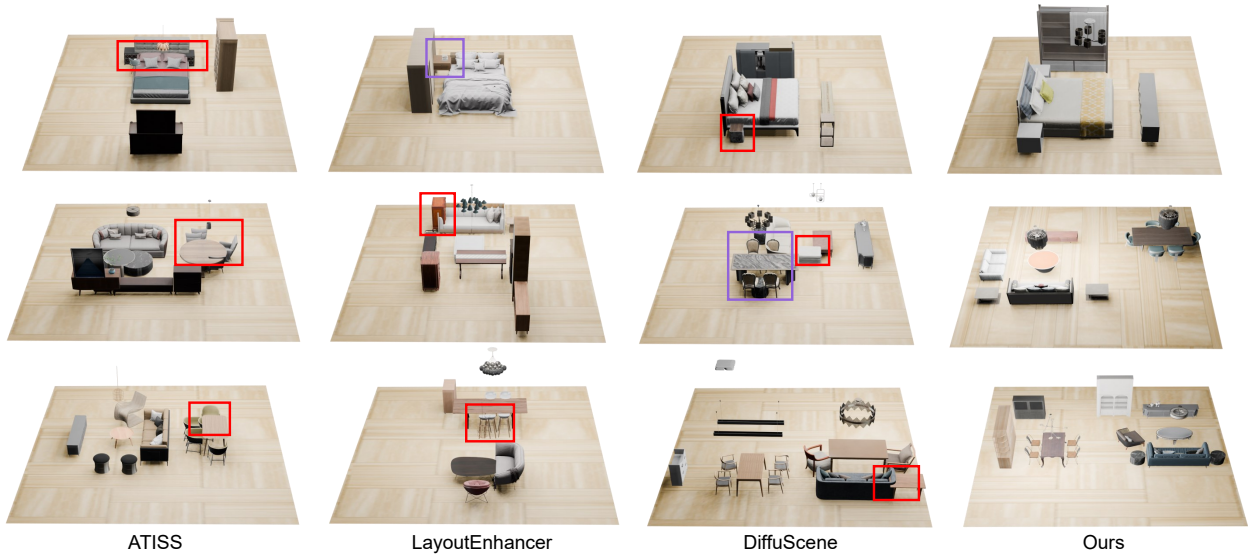


Figure 3. Qualitative results on unconditional layout synthesis. The red boxes indicate overlaps, while the purple boxes highlight unreasonable furniture distribution.

(SCA) and categorical KL Divergence (CKL $\times 0.01$). FID, KID, and SCA are highly sensitive to shape textures and rendering styles. To ensure fairness, we render all competing methods using the same configuration. Following Physcene [56], we adopt Col_{obj}, Col_{scene}, and R_{out} to assess the violation of important spatial relationships. Col_{obj} represents the percentage of objects that collide with others, Col_{scene} denotes the percentage of generated layouts where the object collision occurs. R_{out} evaluates the proportion of objects that extend beyond the floorplan in the floorplanned layout synthesis. For Col_{obj}, Col_{scene}, R_{out}, lower values are better.

We additionally introduce a metric D_{obj} to measure the distribution differences of distance relationships between

frequent object pairs in synthesized layouts and ground truth. A furniture pair is frequent if it appears in more than a specified portion of regions (50% in our experiments). We use Scott’s rule [40] to select the bandwidth for the kernel density estimation plot. At last, D_{obj} takes the averaged differences of the distance expectation between predicted furniture pairs and ground truth ones as the metric. In this way, D_{obj} can effectively assess alterations in the spatial arrangement of the furniture. The distance expectation for all frequent furniture pairs in the ground truth is presented in the supplementary.

Baselines. For indoor layout synthesis, we compare with four state-of-the-art methods: 1) ATISS [34], an autoregressive network for indoor layout generation; 2) Lay-

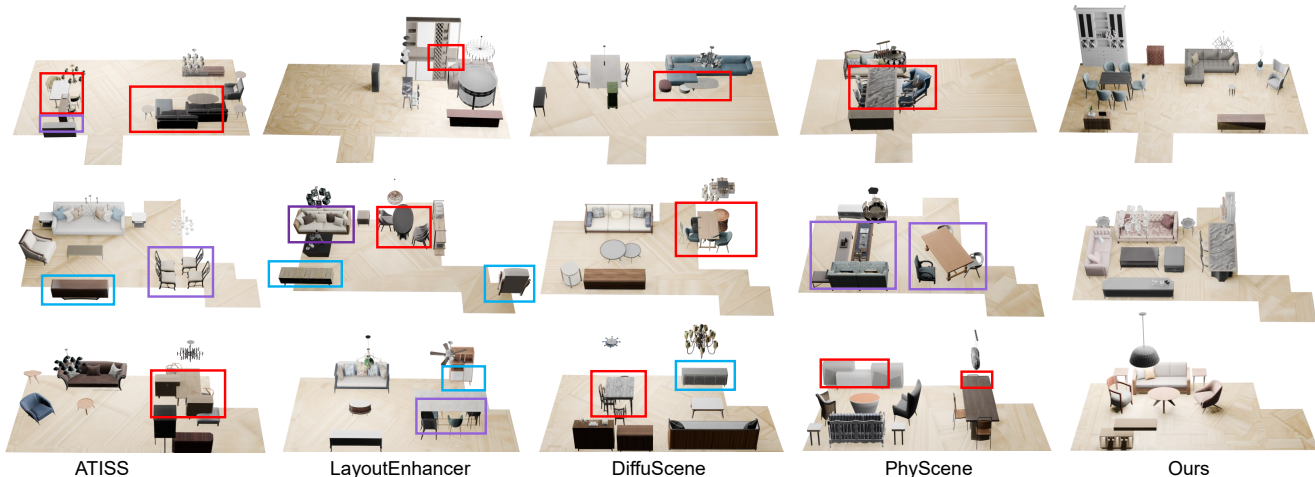


Figure 4. Visualization comparisons of floor-plan conditioned layout synthesis. The red boxes indicate overlap, the blue boxes indicate out-of-bounds, and the purple boxes highlight areas with unreasonable furniture distribution.

Table 2. Quantitative comparisons of floor-conditioned layout synthesis across different models.

Room	Method	FID↓	KID $\times 0.001$ ↓	SCA	CKL $\times 0.01$ ↓	Col _{obj} ↓	Col _{scene} ↓	D _{obj} ↓	R _{out} ↓
Bedroom	ATISS	50.871	2.264	0.533	0.323	0.278	0.593	0.102	0.302
	LayoutEnhancer	48.984	2.143	0.525	0.299	0.247	0.465	0.082	0.276
	Diffuscene	37.060	2.163	0.528	0.312	0.223	0.434	0.056	0.268
	Ours	30.494	1.928	0.518	0.247	0.185	0.382	0.040	0.223
Living room	ATISS	62.920	4.768	0.541	0.212	0.316	0.876	0.771	0.152
	LayoutEnhancer	61.520	4.252	0.535	0.208	0.285	0.874	0.652	0.149
	Diffuscene	49.421	3.546	0.544	0.203	0.254	0.706	0.664	0.248
	PhyScene	50.361	3.632	0.539	0.171	0.202	0.630	0.629	0.220
Ours	47.886	2.278	0.536	0.162	0.187	0.612	0.503	0.224	
Dining room	ATISS	65.136	4.762	0.520	0.316	0.415	0.860	0.571	0.146
	LayoutEnhancer	60.106	3.882	0.518	0.298	0.323	0.824	0.480	0.143
	Diffuscene	48.908	2.889	0.517	0.204	0.185	0.586	0.455	0.202
	Ours	47.865	2.615	0.511	0.178	0.176	0.564	0.398	0.134

Table 3. Quantitative comparisons on the task of scene arrangement in the 3D-FRONT living rooms. We evaluate results with LEGO and DiffuScene as baseline methods. Ours(-) denotes the use of \mathcal{L}_{O2O} and \mathcal{L}_{O2R} .

Method	FID↓	KID $\times 0.001$ ↓	SCA	Col _{obj} ↓	Col _{scene} ↓	D _{obj} ↓
LEGO	66.952	7.592	0.592	0.557	0.898	0.725
Ours (LEGO)	57.290	3.586	0.572	0.397	0.864	0.344
Diffuscene	61.017	5.842	0.586	0.497	0.920	0.495
Ours (Diffuscene)	55.861	2.963	0.575	0.315	0.710	0.292

outEnhancer [24], an autoregressive model incorporating ergonomic and indoor functional design knowledge as a training regularization term; 3) DiffuScene [44], a DDPM-based indoor layout synthesis model that introduces IoU

Table 4. Ablation study on the object-to-object and object-to-region losses.

O2O	O2R	FID↓	KID↓	SCA	CKL↓	Col _{obj} ↓	Col _{scene} ↓	D _{obj} ↓
		51.462	3.925	0.579	0.273	0.254	0.762	0.452
	✓	46.668	1.026	0.519	0.246	0.174	0.550	0.310
✓		46.357	1.246	0.516	0.232	0.174	0.538	0.238
✓	✓	46.216	0.982	0.513	0.218	0.146	0.468	0.222

regularization terms to penalize object collisions; and 4) PhyScene [56], which models pairwise object relationships as a binary classifier and provides classifier guidance for a DDPM-based indoor layout synthesis model. ATISS, DiffuScene, and LayoutEnhancer have released training and inference source code. PhyScene only releases the inference code and the pre-trained model for a floor-conditioned liv-

Table 5. Ablation study of spatial relationship modeling and the regularization implementation.

spt. relationship	reg. term	FID↓	KID×0.001↓	SCA	CKL×0.01↓	Col _{obj} ↓	Col _{scene} ↓	D _{obj} ↓
triple	IoU loss	46.640	1.019	0.519	0.221	0.204	0.626	0.239
	Rendering loss (Ours)	46.216	0.982	0.513	0.218	0.146	0.468	0.222
pairwise	–	47.596	1.029	0.526	0.228	0.193	0.582	0.444

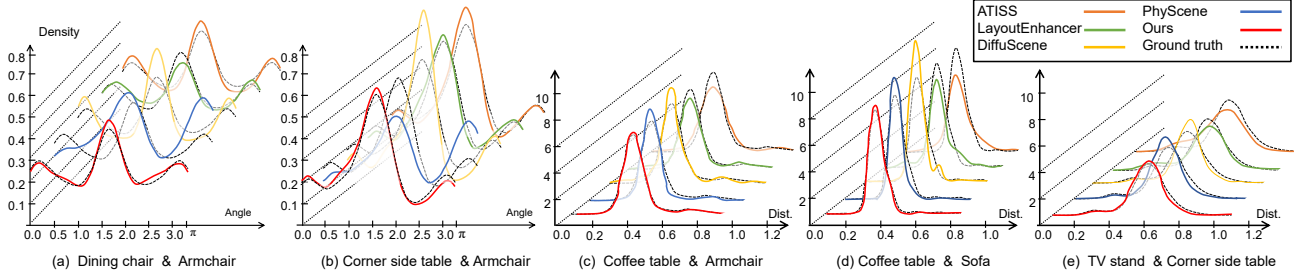


Figure 5. Distribution of the relative distances and angles between object pairs modeled by five approaches—ATISS, LayoutEnhancer, DiffuScene, PhyScene, and Ours—compared to the ground truth, where (a)-(b) visualizes the angle distribution and (c)-(e) visualizes the distance distribution.

ing room. We compare with PhyScene only under this configuration. In addition, we also compare the method with DiffuScene and LEGO [49] for scene rearrangement tasks.

Implementation We train our model using a single NVIDIA A100 GPU, with a batch size of 128, for 100,000 epochs. The initial learning rate was set at 2×10^{-4} and gradually decayed by a factor of 0.5 for every 15,000 epochs. For the diffusion process, we follow the default settings of DDPM [19], where the noise intensity β_t increases linearly from 0.0001 to 0.02 for 1,000 time steps. The complete training for the bedroom, living room, and dining room takes four days. For DBSCAN clustering, epsilon and the min number of samples are set to 1.8 and 2 respectively, with a GIoU weight of $\lambda_{giou} = 0.02$. During training, we set the loss weight $\lambda_{O2O} = 0.05$, $\lambda_{O2R} = 0.025$. To evaluate visual metrics FID, KID and SCA, we construct 3D scenes from the generated indoor layout by retrieving the closest matched CAD furniture from 3D-FUTURE [15] based on the 3D object feature f_i .

4.2. Unconditioned Layout Synthesis

In this scenario, the method directly generates layouts without any input conditions. The quantitative results are presented in Table 1. RelTriple demonstrates a clear advantage across visual quality metrics (FID, KID, SCA, and CKL), showing consistently superior generation quality compared to ATISS, LayoutEnhancer, and DiffuScene. These metrics underscore the effectiveness of incorporating spatial relationships for perceptual and semantic accuracy, which is crucial for generating realistic layouts. In terms of collision metrics, RelTriple significantly reduces object overlaps and boundary violations. For instance, in the living room layout,

RelTriple achieves the best Col_{obj} and Col_{scene} compared to the competing methods. This improvement indicates effective collision management, suggesting that RelTriple is better at collision.

Additionally, RelTriple achieves superior performance in D_{obj}, highlighting its ability to maintain consistent distance relationships. In the bedroom layout, for example, RelTriple achieves a D_{obj} of 0.032, compared to DiffuScene (0.072) and LayoutEnhancer (0.108). This reflects RelTriple’s precision in preserving realistic relative spacing, contributing to both visual authenticity and physical rationality within generated scenes.

Fig. 3 presents a qualitative comparison of different scene synthesis methods. Our generated layouts have fewer object collisions, and the object placement is more reasonable, for example, the proper spacing between a bed and nightstands, a sofa, and its surrounding objects.

4.3. Floor-conditioned Layout Synthesis

In this scenario, the method generates layouts conditioned on a floorplan. Table 2 compares RelTriple with alternative baselines. Note that PhyScene only provided the pre-trained model and testing code for living room comparisons. Across metrics that assess layout realism and spatial organization, RelTriple demonstrates distinct advantages over DiffuScene, LayoutEnhancer, and PhyScene. In the Living Room layout, for example, RelTriple achieves a D_{obj} of 0.503, lower than DiffuScene(0.664) and PhyScene(0.629). This lower D_{obj} value indicates RelTriple’s superior control over object distances, effectively maintaining realistic spacing that contributes to both visual coherence and physical plausibility in the layout.

Although RelTriple’s SCA in the Living Room layout is slightly higher than that of LayoutEnhancer, and its R_{out} is marginally higher than PhyScene and ATISS, these differences likely stem from RelTriple’s prioritization of spatial relationships of indoor objects. RelTriple emphasizes the relationship between objects and regions rather than room boundaries, leading to higher R_{out} but significant improvements in D_{obj} , Col_{obj} , and $\text{Col}_{\text{scene}}$ —metrics that critically affect the layout’s realism and functional utility. In Fig. 5, we provide a kernel density estimate (KDE) plot of the distance distribution between relevant furniture pairs. We can see our method is much closer to the ground truth distribution at both the highest density peak and can accurately track the trends of the overall density changes. Therefore, the generated layouts exhibit more similar distance distributions to the ground truth layouts than other methods. Fig. 4 illustrates a visual comparison between various layout synthesis methods. Our method produces less object obstruction and has less unoccupied space than PhyScene and LayoutEnhancer.



Figure 6. Visual comparisons on scene re-arrangements where the indoor objects are given. The red boxes illustrate incorrect furniture placements, while the green boxes indicate appropriate arrangements.

4.4. Scene Re-arrangement

In this task, we take a set of semantic objects and generate an indoor layout for the living room setting. Table 3 presents the results. We can see the inclusion of RelTriple can greatly improve the performance of both two baselines and achieve better numbers on all metrics, especially for constraint metrics (see improvements in Col_{obj} , $\text{Col}_{\text{scene}}$, and D_{obj}). Qualitative results in Fig 6 show superior performance in avoiding object collisions. We explore the impact of various rotated input layouts on the scene rearrangement produced by RelTriple in the *supplementary*.

4.5. Ablation Studies

In this section, we first evaluate the effectiveness of the proposed two losses. Then we compare the method with two alternative designs for the rendering loss. All experiments are conducted for unconditional living room generation. We leave the hyperparameter analysis and more results to the *supplementary*.

O2O and O2R loss. In Tab. 4, we explore how Object-to-Object (O2O) and Object-to-Region (O2R) loss affect

the generation quality. We evaluate the results of the unconditional generation in living rooms. Comparing row 1 and row 3 in Tab. 4, the O2O loss plays a crucial role in managing important spatial relationships (Col_{obj} 0.254 \rightarrow 0.174, $\text{Col}_{\text{scene}}$ 0.762 \rightarrow 0.538), and shows better distribution of object spacing (D_{obj} 0.452 \rightarrow 0.238), indicating the avoidance of overcrowding or excessive spacing between objects. The O2R loss focuses on fitting objects within designated regions of the indoor layout, ensuring that each object is placed appropriately within the layout. Comparing row 1 and row 2, the generated indoor layout also achieves significant improvements in Col_{obj} (0.254 \rightarrow 0.174), $\text{Col}_{\text{scene}}$ (0.762 \rightarrow 0.550), and D_{obj} (0.452 \rightarrow 0.310). Since O2O and O2R losses focus on distinct indoor layout relationships, and their combination provides the best quantitative results on all metrics.

Alternatives to the Rendering Losses. There are two alternatives for the rendering loss: 1) an IOU-based triple loss that maximizes the intersection over the union between triple triangles of predictions and GTs; 2) a distance-based pairwise loss that minimizes changes in the pairwise distance between two objects in a triple comparing prediction and GT. Results in Table 5 show pairwise distance loss has the worst performance, suggesting the necessity to incorporate high-order triple relations. Furthermore, our rendering loss achieves the best performance among the three choices.

4.6. Limitations

While RelTriple demonstrates significant advancements in generating realistic and constraint-aware indoor layouts, several limitations remain. First, learning 3D spatial relations in 2D spaces may result in unnecessary ambiguity. For example, a TV and a table may overlap in the projected 2D layout. Additionally, the current implementation focuses solely on static furniture arrangements and does not account for dynamic elements or user interactions within the environment.

5. Conclusion

In this paper, we introduced RelTriple, a novel framework for furniture layout generation. We leverage the indoor hierarchy to automatically extract object-to-object and object-to-region relationships and integrate the learning of these relationships into a generative diffusion framework. Our method aims to ensure realistic and functional layouts that respect practical relationships. Experimental results demonstrate that RelTriple outperforms existing methods in a wide variety of metrics. Future work will explore handling dynamic environments by incorporating object movement to support real-time generation, especially for virtual and augmented reality applications.

References

- [1] Sherwin Bahmani, Jeong Joon Park, Despoina Paschalidou, Xingguang Yan, Gordon Wetzstein, Leonidas Guibas, and Andrea Tagliasacchi. Cc3d: Layout-conditioned generation of compositional 3d scenes. In *Proceedings of the IEEE/CVF International Conference on Computer Vision*, pages 7171–7181, 2023. [2](#)
- [2] Mikołaj Bińkowski, Danica J Sutherland, Michael Arbel, and Arthur Gretton. Demystifying mmd gans. *arXiv preprint arXiv:1801.01401*, 2018. [4](#)
- [3] Ata Çelen, Guo Han, Konrad Schindler, Luc Van Gool, Iro Armeni, Anton Obukhov, and Xi Wang. I-design: Personalized llm interior designer. *arXiv preprint arXiv:2404.02838*, 2024. [2](#)
- [4] Aditya Chattopadhyay, Xi Zhang, David Paul Wipf, Himanshu Arora, and René Vidal. Learning graph variational autoencoders with constraints and structured priors for conditional indoor 3d scene generation. In *Proceedings of the IEEE/CVF winter conference on applications of computer vision*, pages 785–794, 2023. [2](#)
- [5] L. Paul Chew. Constrained delaunay triangulations. *Algorithmica*, 4(1):97–108, 1989. [4](#)
- [6] Joseph De Chiara, Julius Panero, and Martin Zelnic. *Time-saver standards for interior design and space planning*. McGraw-Hill, 2001. [2](#)
- [7] Helisa Dhamo, Fabian Manhardt, Nassir Navab, and Federico Tombari. Graph-to-3d: End-to-end generation and manipulation of 3d scenes using scene graphs. In *Proceedings of the IEEE/CVF International Conference on Computer Vision*, pages 16352–16361, 2021. [2](#)
- [8] Prafulla Dhariwal and Alexander Nichol. Diffusion models beat gans on image synthesis. *Advances in neural information processing systems*, 34:8780–8794, 2021. [3](#)
- [9] Yan Ding, Xiaohan Zhang, Chris Paxton, and Shiqi Zhang. Task and motion planning with large language models for object rearrangement. In *2023 IEEE/RSJ International Conference on Intelligent Robots and Systems (IROS)*, pages 2086–2092. IEEE, 2023. [2](#)
- [10] Martin Ester, Hans-Peter Kriegel, Jörg Sander, Xiaowei Xu, et al. A density-based algorithm for discovering clusters in large spatial databases with noise. In *kdd*, pages 226–231, 1996. [4](#)
- [11] Weixi Feng, Wanrong Zhu, Tsu-jui Fu, Varun Jampani, Arjun Akula, Xuehai He, Sugato Basu, Xin Eric Wang, and William Yang Wang. Layoutgpt: Compositional visual planning and generation with large language models. *Advances in Neural Information Processing Systems*, 36, 2024. [2](#)
- [12] David Fernandez-Chaves, Jose-Raul Ruiz-Sarmiento, Alberto Jaenal, Nicolai Petkov, and Javier Gonzalez-Jimenez. Robot@ virtualhome, an ecosystem of virtual environments and tools for realistic indoor robotic simulation. *Expert Systems with Applications*, 208:117970, 2022. [1](#)
- [13] Matthew Fisher, Daniel Ritchie, Manolis Savva, Thomas Funkhouser, and Pat Hanrahan. Example-based synthesis of 3d object arrangements. *ACM Transactions on Graphics (TOG)*, 31(6):1–11, 2012. [1](#)
- [14] Huan Fu, Bowen Cai, Lin Gao, Ling-Xiao Zhang, Jiaming Wang, Cao Li, Qixun Zeng, Chengyue Sun, Rongfei Jia, Binqiang Zhao, et al. 3d-front: 3d furnished rooms with layouts and semantics. In *Proceedings of the IEEE/CVF International Conference on Computer Vision*, pages 10933–10942, 2021. [4](#)
- [15] Huan Fu, Rongfei Jia, Lin Gao, Mingming Gong, Binqiang Zhao, Steve Maybank, and Dacheng Tao. 3d-future: 3d furniture shape with texture. *International Journal of Computer Vision*, 129:3313–3337, 2021. [4](#), [7](#)
- [16] Rao Fu, Zehao Wen, Zichen Liu, and Srinath Sridhar. Any-home: Open-vocabulary generation of structured and textured 3d homes. In *European Conference on Computer Vision*, pages 52–70. Springer, 2024. [2](#)
- [17] Lin Gao, Jia-Mu Sun, Kaichun Mo, Yu-Kun Lai, Leonidas J Guibas, and Jie Yang. Scenehgn: Hierarchical graph networks for 3d indoor scene generation with fine-grained geometry. *IEEE Transactions on Pattern Analysis and Machine Intelligence*, 45(7):8902–8919, 2023. [2](#), [4](#)
- [18] Martin Heusel, Hubert Ramsauer, Thomas Unterthiner, Bernhard Nessler, and Sepp Hochreiter. Gans trained by a two time-scale update rule converge to a local nash equilibrium. *Advances in neural information processing systems*, 30, 2017. [4](#)
- [19] Jonathan Ho, Ajay Jain, and Pieter Abbeel. Denoising diffusion probabilistic models. *Advances in neural information processing systems*, 33:6840–6851, 2020. [7](#)
- [20] Xiaolin Hong, Hongwei Yi, Fazhi He, and Qiong Cao. Human-aware 3d scene generation with spatially-constrained diffusion models. *arXiv preprint arXiv:2406.18159*, 2024. [2](#), [3](#)
- [21] Hiroharu Kato, Yoshitaka Ushiku, and Tatsuya Harada. Neural 3d mesh renderer. In *Proceedings of the IEEE conference on computer vision and pattern recognition*, pages 3907–3916, 2018. [4](#)
- [22] Jing Yu Koh, Harsh Agrawal, Dhruv Batra, Richard Tucker, Austin Waters, Honglak Lee, Yinfei Yang, Jason Baldridge, and Peter Anderson. Simple and effective synthesis of indoor 3d scenes. In *Proceedings of the AAAI Conference on Artificial Intelligence*, pages 1169–1178, 2023. [2](#)
- [23] Alexander Lange. The woman who invented the kitchen. *Slate Magazine*. Retrieved, 592, 2012. [2](#)
- [24] Kurt Leimer, Paul Guerrero, Tomer Weiss, and Przemyslaw Musialski. Layoutenhancer: Generating good indoor layouts from imperfect data. In *SIGGRAPH Asia 2022 Conference Papers*, pages 1–8, 2022. [2](#), [3](#), [6](#)
- [25] Mike Lewis, Yinhan Liu, Naman Goyal, Marjan Ghazvininejad, Abdelrahman Mohamed, Omer Levy, Veselin Stoyanov, and Luke Zettlemoyer. BART: denoising sequence-to-sequence pre-training for natural language generation, translation, and comprehension. *Association for Computational Linguistics*, pages 7871–7880, 2020. [2](#)
- [26] Manyi Li, Akshay Gadi Patil, Kai Xu, Siddhartha Chaudhuri, Owais Khan, Ariel Shamir, Changhe Tu, Baoquan Chen, Daniel Cohen-Or, and Hao Zhang. Grains: Generative recursive autoencoders for indoor scenes. *ACM Transactions on Graphics (TOG)*, 38(2):1–16, 2019. [2](#)

- [27] Chenguo Lin and Yadong Mu. Instructscene: Instruction-driven 3d indoor scene synthesis with semantic graph prior. In *The Twelfth International Conference on Learning Representations*, 2024. 2
- [28] Andrew Luo, Zhoutong Zhang, Jiajun Wu, and Joshua B Tenenbaum. End-to-end optimization of scene layout. In *Proceedings of the IEEE/CVF Conference on Computer Vision and Pattern Recognition*, pages 3754–3763, 2020. 2
- [29] Chuan Ma, Olivia Guerra-Santin, and Masi Mohammadi. Smart home modification design strategies for ageing in place: a systematic review. *Journal of Housing and the Built Environment*, 37(2):625–651, 2022. 1
- [30] Léopold Maillard, Nicolas Sereyjol-Garros, Tom Durand, and Maks Ovsjanikov. Debara: Denoising-based 3d room arrangement generation. *arXiv preprint arXiv:2409.18336*, 2024. 1
- [31] Paul Merrell, Eric Schkufza, Zeyang Li, Maneesh Agrawala, and Vladlen Koltun. Interactive furniture layout using interior design guidelines. *ACM transactions on graphics (TOG)*, 30(4):1–10, 2011. 3
- [32] Yinyu Nie, Angela Dai, Xiaoguang Han, and Matthias Nießner. Learning 3d scene priors with 2d supervision. In *Proceedings of the IEEE/CVF Conference on Computer Vision and Pattern Recognition*, pages 792–802, 2023. 2
- [33] Wamiq Para, Paul Guerrero, Tom Kelly, Leonidas J Guibas, and Peter Wonka. Generative layout modeling using constraint graphs. In *Proceedings of the IEEE/CVF international conference on computer vision*, pages 6690–6700, 2021. 2
- [34] Despoina Paschalidou, Amlan Kar, Maria Shugrina, Karsten Kreis, Andreas Geiger, and Sanja Fidler. Atiss: Autoregressive transformers for indoor scene synthesis. *Advances in Neural Information Processing Systems*, 34:12013–12026, 2021. 1, 2, 5
- [35] Aditya Ramesh, Mikhail Pavlov, Gabriel Goh, Scott Gray, Chelsea Voss, Alec Radford, Mark Chen, and Ilya Sutskever. Zero-shot text-to-image generation. In *International conference on machine learning*, pages 8821–8831. Pmlr, 2021. 2
- [36] Hamid Rezaatoughi, Nathan Tsoi, JunYoung Gwak, Amir Sadeghian, Ian Reid, and Silvio Savarese. Generalized intersection over union: A metric and a loss for bounding box regression. In *Proceedings of the IEEE/CVF conference on computer vision and pattern recognition*, pages 658–666, 2019. 4
- [37] Daniel Ritchie, Kai Wang, and Yu-an Lin. Fast and flexible indoor scene synthesis via deep convolutional generative models. In *Proceedings of the IEEE/CVF Conference on Computer Vision and Pattern Recognition*, pages 6182–6190, 2019. 2
- [38] Robin Rombach, Andreas Blattmann, Dominik Lorenz, Patrick Esser, and Björn Ommer. High-resolution image synthesis with latent diffusion models. In *Proceedings of the IEEE/CVF conference on computer vision and pattern recognition*, pages 10684–10695, 2022. 2
- [39] Peter J Rousseeuw. Silhouettes: a graphical aid to the interpretation and validation of cluster analysis. *Journal of computational and applied mathematics*, 20:53–65, 1987. 3
- [40] David W. Scott. Multivariate density estimation, theory, practice and visualization. *The Statistician*, 43:218–219, 1992. 5
- [41] Ruben M Smelik, Tim Tutenel, Rafael Bidarra, and Bedrich Benes. A survey on procedural modelling for virtual worlds. In *Computer graphics forum*, pages 31–50. Wiley Online Library, 2014. 1
- [42] Jia-Mu Sun, Jie Yang, Kaichun Mo, Yu-Kun Lai, Leonidas Guibas, and Lin Gao. Haisor: Human-aware indoor scene optimization via deep reinforcement learning. *ACM Transactions on Graphics*, 43(2):1–17, 2024. 2, 3
- [43] Hou In Ivan Tam, Hou In Derek Pun, Austin T Wang, Angel X Chang, and Manolis Savva. Scenemotifcoder: Example-driven visual program learning for generating 3d object arrangements. *arXiv preprint arXiv:2408.02211*, 2024. 2
- [44] Jiapeng Tang, Yinyu Nie, Lev Markhasin, Angela Dai, Justus Thies, and Matthias Nießner. Diffuscene: Denoising diffusion models for generative indoor scene synthesis. In *Proceedings of the IEEE/CVF conference on computer vision and pattern recognition*, pages 20507–20518, 2024. 2, 3, 4, 6
- [45] Ashish Vaswani, Noam Shazeer, Niki Parmar, Jakob Uszkoreit, Llion Jones, Aidan N. Gomez, Lukasz Kaiser, and Illia Polosukhin. Attention is all you need. In *Advances in Neural Information Processing Systems 30: Annual Conference on Neural Information Processing Systems 2017, December 4-9, 2017, Long Beach, CA, USA*, pages 5998–6008, 2017. 3
- [46] Can Wang, Hongliang Zhong, Menglei Chai, Mingming He, Dongdong Chen, and Jing Liao. Chat2layout: Interactive 3d furniture layout with a multimodal llm. *arXiv preprint arXiv:2407.21333*, 2024. 2
- [47] Kai Wang, Yu-An Lin, Ben Weissmann, Manolis Savva, Angel X Chang, and Daniel Ritchie. Planit: Planning and instantiating indoor scenes with relation graph and spatial prior networks. *ACM Transactions on Graphics (TOG)*, 38(4):1–15, 2019. 2
- [48] Xinpeng Wang, Chandan Yeshwanth, and Matthias Nießner. Sceneformer: Indoor scene generation with transformers. In *2021 International Conference on 3D Vision (3DV)*, pages 106–115. IEEE, 2021. 1, 2
- [49] Qihong Anna Wei, Sijie Ding, Jeong Joon Park, Rahul Sajnani, Adrien Poulénard, Srinath Sridhar, and Leonidas Guibas. Lego-net: Learning regular rearrangements of objects in rooms. In *Proceedings of the IEEE/CVF Conference on Computer Vision and Pattern Recognition*, pages 19037–19047, 2023. 1, 2, 7
- [50] Yao Wei, Martin Renqiang Min, George Vosselman, Li Erran Li, and Michael Ying Yang. Compositional 3d scene synthesis with scene graph guided layout-shape generation. *arXiv preprint arXiv:2403.12848*, 2024. 2
- [51] Tomer Weiss, Alan Litteneker, Noah Duncan, Masaki Nakada, Chenfanfu Jiang, Lap-Fai Yu, and Demetri Terzopoulos. Fast and scalable position-based layout synthesis. *IEEE Transactions on Visualization and Computer Graphics*, 25(12):3231–3243, 2018. 3
- [52] Christopher D Wickens and C Melody Carswell. The proximity compatibility principle: Its psychological foundation

and relevance to display design. *Human factors*, 37(3):473–494, 1995. 4

- [53] Rui Xu, Le Hui, Yuehui Han, Jianjun Qian, and Jin Xie. Scene graph masked variational autoencoders for 3d scene generation. In *Proceedings of the 31st ACM International Conference on Multimedia*, pages 5725–5733, 2023. 2
- [54] Yinghao Xu, Menglei Chai, Zifan Shi, Sida Peng, Ivan Skokhodov, Aliaksandr Siarohin, Ceyuan Yang, Yujun Shen, Hsin-Ying Lee, Bolei Zhou, et al. Discoscene: Spatially disentangled generative radiance fields for controllable 3d-aware scene synthesis. In *Proceedings of the IEEE/CVF conference on computer vision and pattern recognition*, pages 4402–4412, 2023. 2
- [55] Ming-Jia Yang, Yu-Xiao Guo, Bin Zhou, and Xin Tong. Indoor scene generation from a collection of semantic-segmented depth images. In *Proceedings of the IEEE/CVF International Conference on Computer Vision*, pages 15203–15212, 2021. 2
- [56] Yandan Yang, Baoxiong Jia, Peiyuan Zhi, and Siyuan Huang. Physcene: Physically interactable 3d scene synthesis for embodied ai. In *Proceedings of the IEEE/CVF Conference on Computer Vision and Pattern Recognition*, pages 16262–16272, 2024. 2, 3, 4, 5, 6
- [57] Yixuan Yang, Junru Lu, Zixiang Zhao, Zhen Luo, James JQ Yu, Victor Sanchez, and Feng Zheng. Llplace: The 3d indoor scene layout generation and editing via large language model. *arXiv preprint arXiv:2406.03866*, 2024. 2
- [58] Yi-Ting Yeh, Lingfeng Yang, Matthew Watson, Noah D Goodman, and Pat Hanrahan. Synthesizing open worlds with constraints using locally annealed reversible jump mcmc. *ACM Transactions on Graphics (TOG)*, 31(4):1–11, 2012. 3
- [59] Lap Fai Yu, Sai Kit Yeung, Chi Keung Tang, Demetri Terzopoulos, Tony F Chan, and Stanley J Osher. Make it home: automatic optimization of furniture arrangement. *ACM Transactions on Graphics (TOG)*, 30(4), 2011. 3
- [60] Guangyao Zhai, Evin Pinar Örnek, Shun-Cheng Wu, Yan Di, Federico Tombari, Nassir Navab, and Benjamin Busam. Commonsences: Generating commonsense 3d indoor scenes with scene graphs. *Advances in Neural Information Processing Systems*, 36, 2023. 2
- [61] Guangyao Zhai, Evin Pinar Örnek, Dave Zhenyu Chen, Ruotong Liao, Yan Di, Nassir Navab, Federico Tombari, and Benjamin Busam. Echoscene: Indoor scene generation via information echo over scene graph diffusion. In *European Conference on Computer Vision*, pages 167–184. Springer, 2024. 2
- [62] Song-Hai Zhang, Shao-Kui Zhang, Wei-Yu Xie, Cheng-Yang Luo, Yong-Liang Yang, and Hongbo Fu. Fast 3d indoor scene synthesis by learning spatial relation priors of objects. *IEEE Transactions on Visualization and Computer Graphics*, 28(9):3082–3092, 2021. 3

RelTriple: Learning Plausible Indoor Layouts by Integrating Relationship Triples into the Diffusion Process

Supplementary Material

In this supplementary material, we provide additional analysis of our methodology, including discussions on balancing weights for losses in Section A, visualizations of the ablation study on relationships in Section B, additional visual results in Section C, analysis of clustering parameters in Section D, discussions on possible extensions in Section E, and statistical analysis of frequent object pairs in Section F.

A. Discussions on Loss Weights

We analyzed the balancing weights between Object-to-Object (O2O) and Object-to-Region (O2R) relationships with respect to the D_{obj} and Col_{obj} metrics. Figure A.7 (a) demonstrates that both D_{obj} and Col_{obj} achieve optimal furniture placement when the weight of O2O losses is approximately 0.05. Deviating from this weight, either higher (e.g., 0.06) or lower (e.g., 0.04), increases metric values, indicating less optimal results. For the O2R loss, Figure A.7 (b) shows that weights around 0.025 yield the best overall distribution of furniture. Conversely, excessively high (e.g., 0.045) or low (e.g., 0.005) weights lead to elevated D_{obj} and Col_{obj} values, reflecting less desirable layout outcomes.

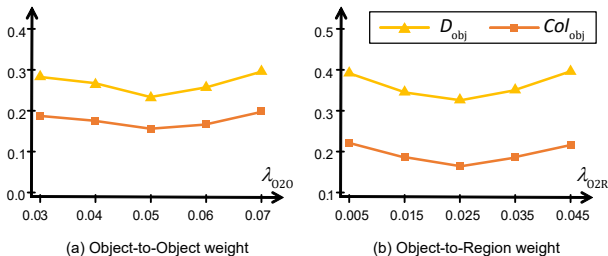


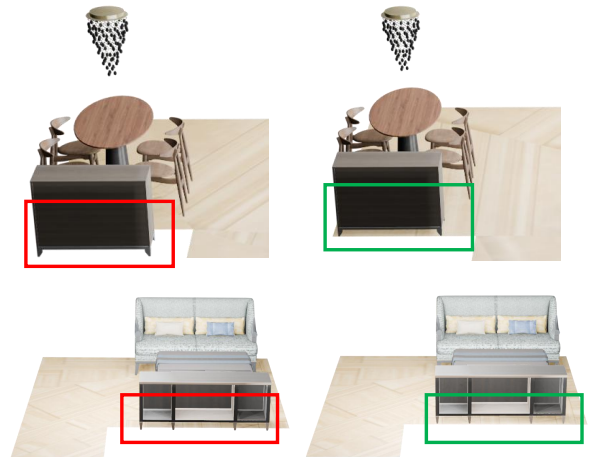
Figure A.7. Evaluations on the varying weights for loss balancing.

B. Ablation Study

We provide qualitative visualizations illustrating the effect of each constraint in Figure A.8. The concepts of O2O and O2R relationships are essential for generating plausible indoor layouts. O2O relationships focus on interactions among sets of three objects, promoting realistic spatial groupings, avoiding collisions, and maintaining proper functional spacing. For example, in a living room, these relationships might ensure a sofa, coffee table, and TV stand are positioned logically relative to each other. On the other hand, O2R relationships involve the alignment of in-



(a) Visual evaluation of O2O constraint.



(b) Visual evaluation of O2R constraint.

Figure A.8. Ablation study visualization results. The boxes in red highlight unreasonable furniture arrangements, while the boxes in green indicate the furniture layout after adding relationships. By introducing relationships, we maintain reasonable spacing between furniture, resulting in a layout that is more physically realistic.

dividual objects with room regions, such as ensuring furniture respects region boundaries or clusters within functional zones. These enhancements outperform state-of-the-art methods by directly modeling spatial relationships via clustering, constrained Delaunay triangulation, and specialized loss functions during training.

C. More Qualitative Results

C.1. Unconditional Layout Synthesis

We present additional visual examples generated by our unconditional layout synthesis model in Figure A.9. Red boxes indicate overlapping furniture, while purple boxes highlight unreasonable furniture arrangements.

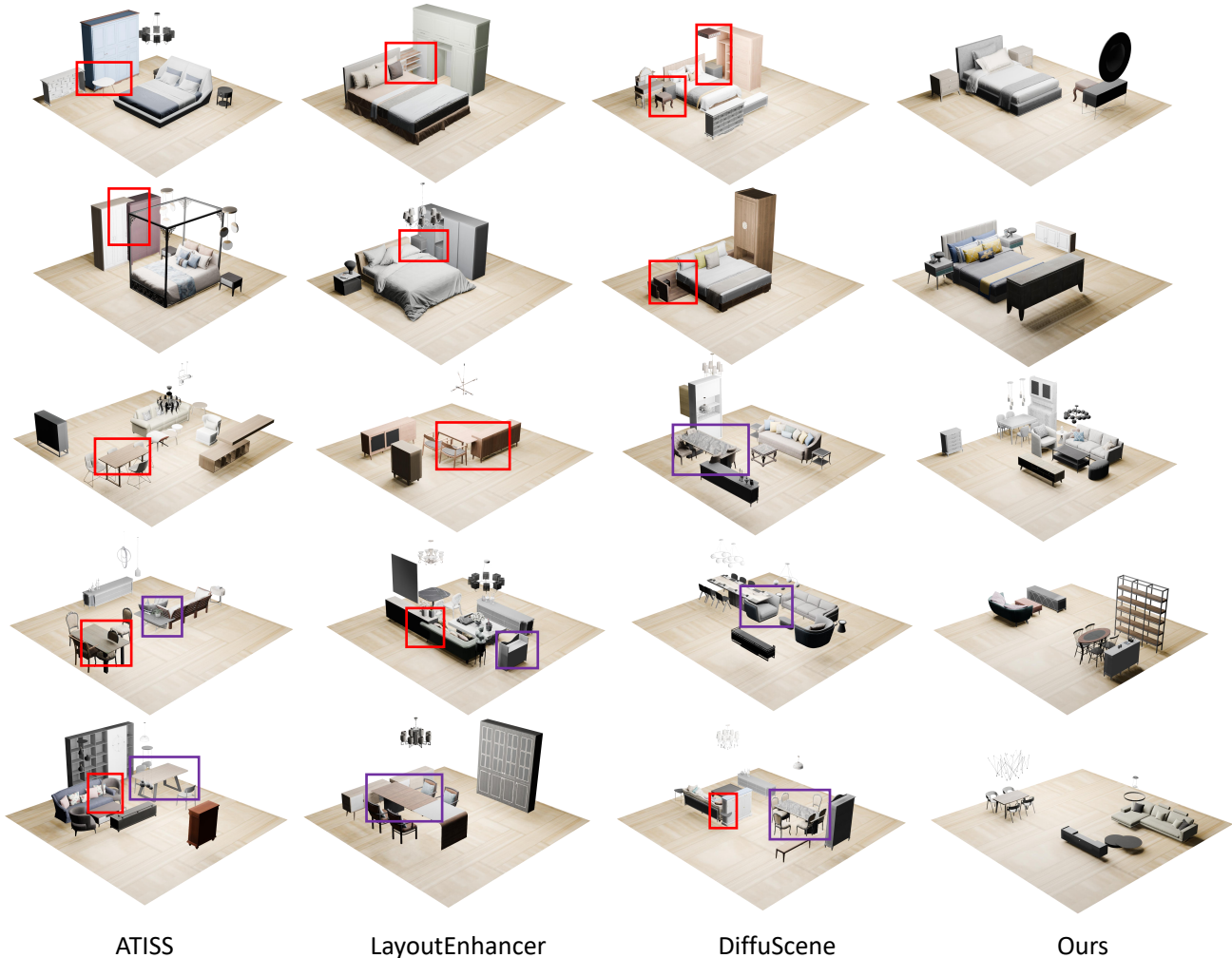


Figure A.9. Qualitative results on unconditional layout synthesis. The red boxes mark furniture overlaps and the purple boxes indicate improper furniture arrangements.

C.2. Floor-conditioned Layout Synthesis

In Figure A.10, we present additional visualization results of floor-conditioned layout synthesis. For a clearer comparison, red boxes highlight overlapping furniture, blue boxes indicate boundary violation, and purple boxes denote unreasonable furniture arrangements. Compared to ATISS [34], LayoutEnhancer [24], DiffuScene [44], and PhyScene [56], our method achieves more reasonable and well-balanced furniture distributions.

C.3. Scene Re-arrangement

In the rearrangement task, we incorporate the relational rendering loss into two baselines, DiffuScene [44] and LEGO [49]. Figure A.11 and Figure A.12 illustrate the visualization results, where red boxes highlight unreasonable furniture arrangements and green boxes showcase the im-

proved counterparts. The relational rendering loss can be integrated into various frameworks, enhancing the physical realism of generated scenes.

C.4. The Impact of Layout Rotations

To evaluate the impact of rotating the input layout, we sequentially rotated the test inputs by 90 degrees in a clockwise direction. We used living room data for testing in the task of scene rearrangement. The visual comparison between the generated layouts is presented in Figure A.13. The quantitative results are presented in Table A.6. The changes in the two metrics, D_{obj} (0.292 \rightarrow 0.308 \rightarrow 0.303 \rightarrow 0.288) and Col_{obj} (0.315 \rightarrow 0.318 \rightarrow 0.322 \rightarrow 0.310) indicates that rotating the layout has some slight impacts on the results.

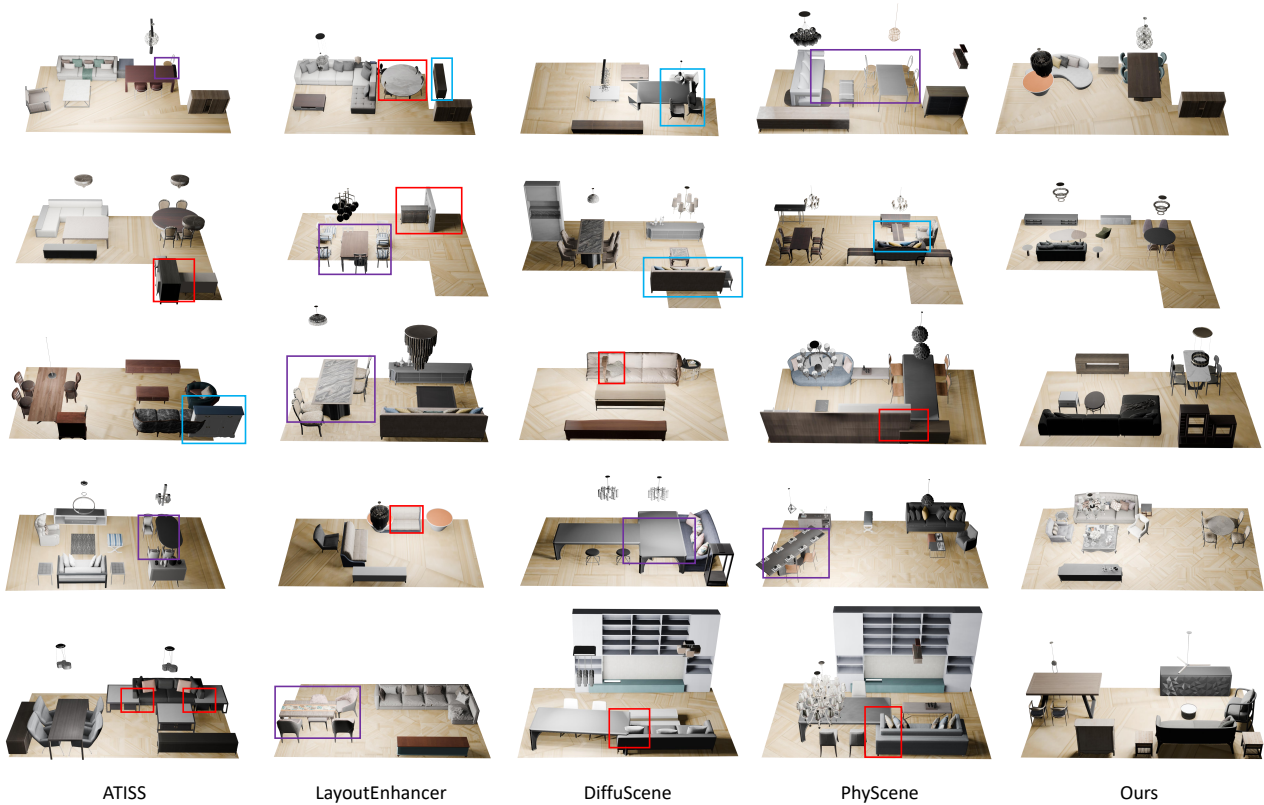


Figure A.10. Visualization comparisons of floor-plan conditioned layout synthesis. Overlapping furniture is marked with red boxes, out-of-bounds areas are highlighted in blue boxes, and regions with unreasonable furniture arrangements are indicated with purple boxes.

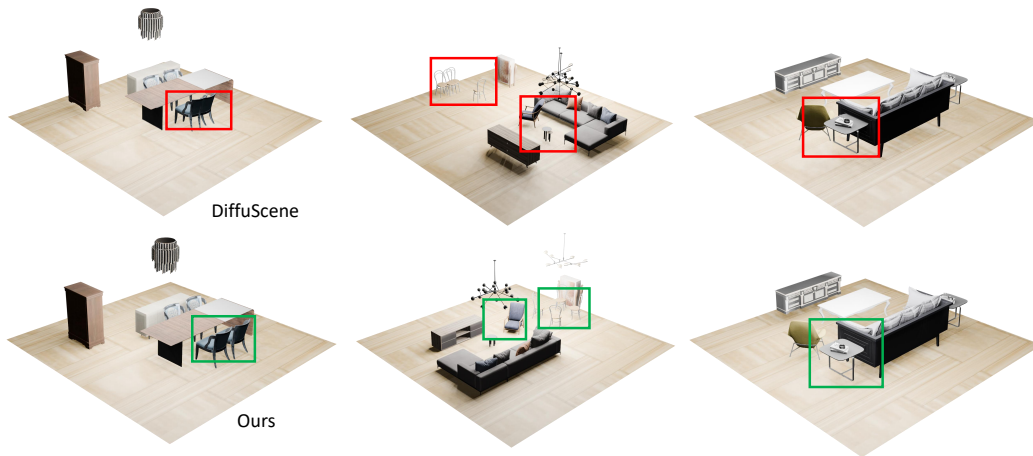


Figure A.11. The visual results of scene rearrangement are presented based on the DiffuScene baseline. Furniture arranged incorrectly is highlighted with red boxes, while correctly arranged furniture is marked with green.

D. Cluster HyperParameters

Following the unsupervised evaluation of DBSCAN, we take the silhouette score for evaluation (see [39] for the definition). A higher silhouette score relates to a model with

better-defined clusters. As shown in Figure A.14, if ϵ is set too high (e.g., approaching boundary values such as 3.8), it results in an over-merging of data points into fewer clusters, which diminishes the precision and distinctiveness of the clusters. Conversely, an excessively low ϵ value (e.g.,

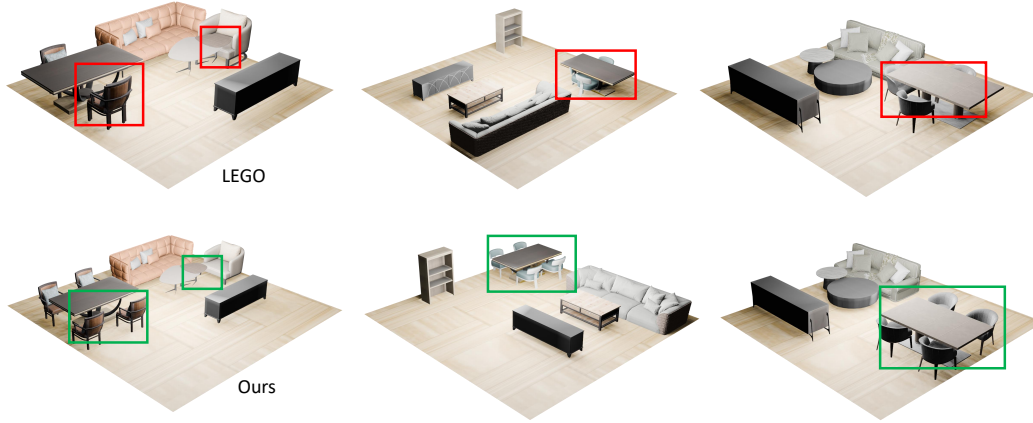


Figure A.12. The visual results of scene rearrangement, based on the LEGO baseline, show incorrectly arranged furniture marked with red boxes, while correctly arranged objects are highlighted in green.



Figure A.13. In the scene rearrangement task, we rotate the input layout clockwise to evaluate the method’s robustness to rotational transformations.

Table A.6. To test the robustness to rotation, the input layout is rotated clockwise by 90 degrees sequentially.

Metric	FID↓	KID↓	SCA	Col _{obj} ↓	Col _{scene} ↓	D _{obj} ↓
0	55.861	2.963	0.575	0.315	0.710	0.292
90	54.918	3.009	0.568	0.318	0.715	0.308
180	56.174	3.072	0.577	0.322	0.692	0.303
270	54.383	2.896	0.574	0.310	0.705	0.288

below 0.8) may lead to over-segmentation, causing the generation of numerous isolated points or fragmented clusters. Setting the value to 1.8 strikes an optimal balance between

grouping related data points and handling sparse regions effectively. Additionally, the minimum number of samples is set to 2. This is because furniture relationships take at least two objects. A larger minimum number of samples is possible and will ignore meaningful pairwise relationships, making it not a good choice.

E. Potential Extensions to Other Constraints

The proposed relationship loss can be further extended to avoid boundary violations and incorporate human functionality. For boundary violations, we can include boundary points as nodes for Delaunay Triangulation, therefore spac-

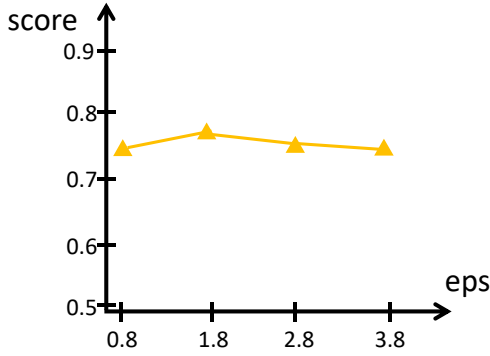


Figure A.14. Impact of the ϵ parameter on DBSCAN clustering results.

ing between furniture and layout boundary can be properly learned. For human functionality, humans can be treated as dynamic nodes in the spatial graph. By incorporating human motion sequences into the relationship modeling process, triple relationships can be introduced. For example, using Delaunay Triangulation, human motion trajectories can act as anchor points that dynamically influence the relative placement of nearby objects. This allows the model to better preserve pathways, maintain ergonomic spacing, and ensure that furniture arrangements adapt to human activities. By leveraging these triple relationships, the generated 3D scenes align more naturally with human-centric functionality. We will explore this direction for future research.

F. Frequent Object Pairs

In Table A.7, we present the frequent furniture pairs and their average distances. The statistical average distances are used to calculate D_{obj} .

Table A.7. Furniture Distance Statistics

Room	Furniture Pair	Average Distance
Dining room	cabinet - dining_chair	0.524
	dining_chair - dining_table	0.176
	corner_side.table - dining_table	0.745
	coffee_table - dining_table	0.689
	coffee_table - corner_side.table	0.397
	console.table - dining_chair	0.475
	dining_chair - dining_chair	0.244
	dining_chair - multi_seat_sofa	0.734
	armchair - dining_chair	0.832
	coffee_table - dining_chair	0.720
	dining_chair - tv_stand	0.779
	coffee_table - tv_stand	0.371
	dining_chair - loveseat_sofa	0.795
	corner_side.table - dining_chair	0.774
bookshelf - dining_chair	0.541	
dining_chair - wine_cabinet	0.459	
dining_chair - stool	0.526	
Bedroom	double_bed - wardrobe	0.730
	nightstand - wardrobe	0.882
	double_bed - nightstand	0.571
	nightstand - nightstand	0.907
Living room	coffee_table - multi_seat_sofa	0.256
	corner_side.table - multi_seat_sofa	0.315
	armchair - coffee_table	0.301
	armchair - corner_side.table	0.418
	coffee_table - corner_side.table	0.405
	coffee_table - dining_table	0.689
	dining_chair - dining_table	0.173
	dining_chair - dining_chair	0.231
	dining_chair - loveseat_sofa	0.784
	coffee_table - tv_stand	0.366
	corner_side.table - tv_stand	0.638
	coffee_table - dining_chair	0.719
	dining_table - tv_stand	0.723
	corner_side.table - dining_table	0.735
	dining_chair - tv_stand	0.757
	corner_side.table - dining_chair	0.767
	bookshelf - dining_chair	0.526
	dining_chair - multi_seat_sofa	0.742
	armchair - dining_chair	0.822
	dining_chair - wine_cabinet	0.493
	console.table - dining_chair	0.483
	dining_chair - stool	0.571
	cabinet - dining_chair	0.568
dining_chair - lounge_chair	0.797	